Co-MOF-derived core-shell $CoP@Co_3O_4$ nanoparticle loaded N-doped graphene: An efficient catalyst for oxygen evolution reaction

Xian-Chen Meng,[a] Jian Luan,[a*] Yi Liu,[a] Yu-Shu Sheng,[a] Fu-Yu Guo,[a] Peng Zheng,[b] Wen-Long Duan,[a*] and Wen-Ze Li[a*]

[a] *College of Science, Shenyang University of Chemical Technology, Shenyang, 110142, P. R. China*

[b] *Key Laboratory on Resources Chemicals and Materials of Ministry of Education, Shenyang University of Chemical Technology, Shenyang, 110142, P. R. China*

E-mails: jluan@syuct.edu.cn (J. Luan); wlduan@syuct.edu.cn (W. L. Duan); wzli@syuct.edu.cn (W. Z. Li)

S1. Experimental section

S1.1 Materials and methods.

The 3-dpyb was synthesized according to the method reported in another literature.[1] Other chemicals and reagents purchased from commercial sources without further processing for purification were utilized for synthesis of MOFs and their pyrolysis products.

S1.2 Preparation of Co-MOFs.

S1.2.1 Synthesis of $\{[Co(3\text{-dpyb})(1,3\text{-BDC})]\cdot H_2O\}_n$ (Co-MOF-H).

In a 25 mL Teflon-lined autoclave, a combination of $CoCl_2\cdot 6H_2O$ (0.047 g, 0.20 mmol), 3-dpyb (0.030 g, 0.10 mmol), 1,3-BDC (0.025 g, 0.15 mmol), NaOH (0.008 g, 0.20 mmol), and H_2O (6 mL) was heated at 120 °C for 4 days. Following that, the mixture in the autoclave was naturally cooled to room temperature, resulting in the formation of purple block crystals of Co-MOF-H (44% yield based on Co). Theoretical values of elemental analysis for $C_{24}H_{24}CoN_4O_7$ (%): C, 53.44; N, 10.39; H, 4.48; found: C, 53.44; N, 10.38; H, 4.48. FTIR (KBr, cm^{-1}): 3110 (s), 1680 (w), 1650 (m), 1611 (m), 1570 (m), 1470 (m), 1400 (s), 1320 (w), 1160 (w), 1110 (w), 1070 (w), 1040 (w), 831 (w), 744 (w), 721 (w), 700 (w), 646 (w).

S1.2.2 Synthesis of {[Co(3-dpyb)(5-MIP)]·H_2O}$_n$ (Co-MOF-CH_3).

To synthesize Co-MOF-CH_3, use the same procedure as for Co-MOF-H, except for replacing 1,3-H_2BDC to 5-H_2MIP (0.027 g, 0.15 mmol). Purple block crystals of Co-MOF-CH_3 were obtained in 27% yield based on Co. Theoretical values of elemental analysis for $C_{25}H_{26}CoN_4O_7$ (%): C, 54.25; N, 10.12; H, 4.74; found: C, 54.25; N, 10.13; H, 4.72. FTIR (KBr, cm^{-1}): 3110 (s), 1680 (m), 1640(m) , 1590 (m), 1540 (m), 1422 (m), 1400 (s), 1320 (w), 1250 (w), 1200 (w), 1160 (w), 1110 (w), 1040 (w), 930 (w), 839 (w), 796 (w), 773 (w), 725 (w), 700 (w), 646 (w), 600 (w).

S1.2.3 Synthesis of {[Co_2(3-dpyb)$_2$(5-HIP)$_2$]·11H_2O}$_n$ (Co-MOF-OH).

To synthesize Co-MOF-OH, use the same procedure as for Co-MOF-H, except for replacing 1,3-H_2BDC to 5-H_2HIP (0.027 g, 0.15 mmol). Purple block crystals of Co-MOF-OH were obtained in 42% yield based on Co. Theoretical values of elemental analysis for $C_{48}H_{66}Co_2N_8O_{25}$ (%): C, 45.29; N, 8.80; H, 5.23; found: C, 45.28; N, 8.79; H, 5.22. FTIR (KBr, cm^{-1}): 3120 (s), 1640 (w), 1580 (w), 1400 (s), 791 (w), 723 (w), 702 (w).

S1.2.4 Synthesis of {[Co_3(3-dpyb)$_3$(5-SIP)$_2$(H_2O)$_8$]·4H_2O}$_n$ (Co-MOF-SO_3).

To synthesize Co-MOF-SO_3, use the same procedure as for Co-MOF-H, except for replacing 1,3-H_2BDC to 5-H_3SIP (0.037 g, 0.15 mmol). Pink block crystals of Co-MOF-SO_3 were obtained in 21% yield based on Co. Theoretical values of elemental analysis for $C_{64}H_{84}Co_3N_{12}O_{32}S_2$ (%): C, 43.32; N, 9.48; H, 4.77; found: C, 43.32; N, 9.48; H, 4.77. FTIR (KBr, cm^{-1}): 3120 (s), 1610 (m), 1600 (m), 1550 (m), 1480 (w), 1400 (s), 1210 (w), 1190 (w), 1110 (w), 1040 (w), 785 (w), 706(w), 629(w).

S1.2.5 Synthesis of {[Co(3-dpyb)(5-NIP)]·H_2O}$_n$ (Co-MOF-NO_2).

To synthesize Co-MOF-NO_2, use the same procedure as for Co-MOF-H, except for replacing 1,3-H_2BDC to 5-H_2NIP (0.031 g, 0.15 mmol). Pink block crystals of Co-MOF-NO_2 were obtained in 36% yield based on Co. Theoretical values of elemental analysis for $C_{24}H_{23}CoN_5O_9$ (%): C, 49.32; N, 11.99; H, 3.97; found: C, 49.31; N, 11.96; H, 3.95. FTIR (KBr, cm^{-1}): 3120 (s), 1630 (s), 1540 (s), 1460 (m), 1400 (s), 1350 (w), 1320 (w), 1200 (w), 1160 (w), 1110 (w), 1080 (w), 1040(w), 926 (w), 874 (w), 829 (w), 789 (w), 735 (m), 717 (m), 702 (m), 646 (w).

S2. Characterization

Crystallographic data for Co-MOF-H, Co-MOF-CH_3, Co-MOF-OH, Co-MOF-SO_3, Co-MOF-NH_2 and Co-MOF-NO_2 were collected using a Bruker SMART APEX II. All structures were resolved using the SHELXTL software.[2] Table S1 summarized the crystal parameters, the data collecting parameters, and the refinement data. Tables S2-S7 listed the selected bond distances and bond angles. CCDC numbers: 988387, 2361269-2361273 for Co-MOF-H, Co-MOF-CH_3, Co-MOF-OH, Co-MOF-SO_3, Co-MOF-NH_2 and Co-MOF-NO_2 can be obtained via www.ccdc.cam.ac.uk/data_request/cif. The elemental analyses (C, H, and N) were determined with the use of a Perkin-Elmer 240C elemental analyzer. FTIR spectra (KBr pellets) were recorded with a Varian 640-IR spectrometer over the range of 4000–500 cm^{-1}. The thermogravimetric analysis (TGA) experiments were performed using a PerkinElmer TGA analyzer. Powder X-ray diffraction (PXRD) data was collected using a Bruker D8 ADVANCE with CuKα radiation to study phase purity and crystal structure by scanning within 2θ range of 5°-90°, step size 3°/min. The external texture and shape of the carbon samples were characterized by scanning electron microscopy (FESEM, *JSM-IT800, JEOL) and high resolution transmission electron microscopy (HRTEM, JEOL2010 at 200 kV). Laser Raman spectroscopy was used to estimate the quality of the carbon-based materials. X-ray photoelectron spectroscopy (XPS) was performed using an Escalab 250 with an Al Kα radiation.The Renishaw inVia Raman spectrometer cooperated with Ar-ion laser of 633 nm wavelength is used to investigate Raman scattering signals.Specific surface area and pore size distribution of samples were identified by nitrogen adsorption/desorption at 77 K using a BUILDER SSA-6000 instrument according to the Barrett-Joyner-Halenda (BJH) method.

S3. Electrochemical measurements

The OER catalytic performance were determined with a CHI 660E electrochemical

workstation (CHI 660E, Shanghai, China). Adopt the system of three-electrode to evaluate the electrochemical activity of commercial catalyst (RuO_2) and the materials of Co-MOF-C serials. Co-MOF-C (5 mg), ethanol (1 mL), Nafion (30 μL) were mixed in room temperature by ultrasonication for 30 min respectively to prepare the catalyst ink. And a glassy carbon electrode with a diameter of 3.0 mm, graphite rod and HgO/Hg electrode were used as the working electrode, counter electrode and reference electrode, respectively. 3 μL catalyst ink was dripped on the glassy carbon electrode polished with Al_2O_3 (1 μm, 0.3 μm and 0.05 μm) to form a thin film with the catalyst loading of 0.2 mg cm^{-2} and naturally dried at room temperature to prepare the working electrode. The commercial RuO_2 catalyst powder was prepared using the same method. And all the electrochemical experiments were conducted in 1 M KOH aqueous solution. Linear sweep voltammetry (LSV) was measured at a scan rate of 10 mV s^{-1} and were referenced to the reversible hydrogen electrode (RHE) according to the following equation: $E_{RHE} = E_{HgO/Hg} + E_{HgO/H}$ (reference) + 0.059 × pH. Whereas the value of $E_{HgO/Hg}$ (reference) is 0.098 V, and none of the LSV curves have been iR corrected. Tafel slopes were analyzed according to equation, $\eta = a + b(\log |j|)$. Wherein, a is constant and b is the Tafel slope and j is current density. Electrochemical impedance spectroscopy was determined in a frequency range of 1-10^6 Hz with an amplitude of 5 mV at a given potential. Electrochemical double-layer was calculated by different scan rates of Cyclic voltammetry (CV) measurement at nonfaradaic potential region. The stability of the catalyst was measured by I-t test.

S4. Density functional theory calculations

In this study, we perform density functional theory (DFT) calculations using the Perdew-Burke-Ernzerhof (PBE) formula in generalized gradient approximation (GGA) using first principles.[3, 4] All theoretical calculations were carried out in the Vienna Ab-initio Simulation Package (VASP). The exchange-correlation effects were described by the Perdew-Burke-Ernzerhof (PBE). Projector-Augmented Wave (PAW) pseudopotentials were used to deal with the core valence interactions, and a cutoff

energy of 400 eV was used. The Castep module in MS was used to optimize the energy of the established model. In the optimization of geometric structure, all calculations reached the convergence standard when the energy and force were reduced to 10^{-5} eV and 0.01 eV $Å^{-1}$. The Brillouin zone integration is performed using 1 × 1 × 1 Monkhorst-Pack k-point sampling for a structure. Partial occupancies of the Kohn−Sham orbitals were allowed using the Gaussian smearing method with width of 0.05 eV. The electronic energy was considered self-consistent when the energy change was smaller than 10^{-5} eV. A geometry optimization was considered convergent when the energy change was smaller than 0.03 eV $Å^{-1}$. The vacuum space of 30 Å was chosen to eliminate reactions between plates.

The OER activity of the catalyst was calculated using the computational hydrogen electrode (CHE) model developed by Nørskov et al.[5] Specifically, the OER process involves four elementary steps, as shown below:

$$*+OH^- \rightarrow OH^*+e^- \quad (S1)$$

$$OH^*+OH^- \rightarrow O^*+H_2O+e^- \quad (S2)$$

$$O^*+OH^- \rightarrow OOH^*+e^- \quad (S3)$$

$$OOH^*+OH^- \rightarrow *+O_2+H_2O+e^- \quad (S4)$$

where * is the active site of the catalyst. The Gibbs free energy change (ΔG) of each elementary step can be computed by:

$$\Delta G=\Delta E+\Delta ZPE-T\,\Delta S+\Delta G_U \quad (S5)$$

where ΔE is the calculated binding energy change of the intermediates, ΔZPE and ΔS represent the zero-point and entropy changes of each step. ΔGU = -eU with U representing the applied potential.

S5. Crystal structure of Co-MOFs

Co-MOF-H was proved to the *P*–1 space group of the triclinic system by crystallographic analysis. The centre metal ion Co(II) connected to two pyridine N atom from two 3-dpyb ligands and four O atoms of three 1,3-BDC anions (Fig. S1a). Wherein, the bond of lengths Co–O and Co–N are in the range of 2.0321(19)–2.312(2)

Å, which are all belonging to the normal ranges. And the two carboxyl of 1,3-BDC anions show two different coordination forms. One 1,3-BDC anion coordinates to three Co(II) ions, which constitute a 1D $[Co(1,3\text{-}BDC)]_{2n}$ chain (Fig. S1b). Moreover, the 3-dpyb ligands show a bis(monodentate) bridging coordination mode, which link by Co(II) ions to generate a 1D *meso*-helical $[Co(3\text{-}dpyb)]_n$ chain (Fig. S1c). Such *meso*-helical $[Co(3\text{-}dpyb)]_n$ chains bridge the adjacent $[Co(1,3\text{-}BDC)]_{2n}$ chains to generate a 2D framework (Fig. S1d). From the topological view, if each binuclear Co cluster is considered as a 4-connected node and the 1,3-BDC anions and 3-dpyb ligands are considered as linkers, the structure of Co-MOF can be simplified as a sql network (Fig. 1e).

Crystal structure of Co-MOF-CH_3 was exhibited in Fig. S2, which is same as the structure of Co-MOF-H, except for the bond of lengths Co–O and Co–N are in the range of 2.0265(17)–2.352(2) Å.

Crystal structure of Co-MOF-OH was exhibited in Fig. S3, which is same as the structure of Co-MOF-H, except for the bond of lengths Co–O and Co–N are in the range of 2.011(3)–2.344(3) Å. Notably, the 2D framework of the structure contains polynuclear water clusters.

Crystal structure of Co-MOF-NO_2 was exhibited in Fig. S4, which is same as the structure of Co-MOF-H, except for the bond of lengths Co–O and Co–N are in the range of 2.031(4)–2.295(4) Å.

Co-MOF-SO_3 was proved to the *P*–1 space group of the triclinic system by crystallographic analysis. Two crystallographically independent Co(II) ions are connected to two pyridine N atom from two 3-dpyb ligands and one O atoms of one 5-SIP anions and three coordinated water molecules (Figs. S5a and S5b). Wherein, the bond of lengths Co–O and Co–N are in the range of 2.0640(19)–2.179(2) Å, which are all belonging to the normal ranges. In this structure, one 5-SIP anion coordinates to two Co(II) ions, which constitute a $Co_3(5\text{-}SIP)_2$ trinuclear unit (Fig. S5c). Moreover, the 3-dpyb ligands show a bis(monodentate) bridging coordination mode, which link by Co(II) ions to generate a 1D zigzag $[Co(3\text{-}dpyb)]_n$ chain (Fig. S5d). Such zigzag $[Co(3\text{-}dpyb)]_n$ chains bridge the adjacent $Co_3(5\text{-}SIP)_2$ chains to

generate a 2D framework (Fig. S5e). From the topological view, if Co(II) ion is considered as a 3/4-connected node and the 5-SIP anions and 3-dpyb ligands are considered as linkers, the structure of Co-MOF-SO_3 can be simplified as a 3,4-connected network with $(4\cdot6^2)_2(4^2\cdot6^2\cdot8^2)$ topology (Fig. S5f).

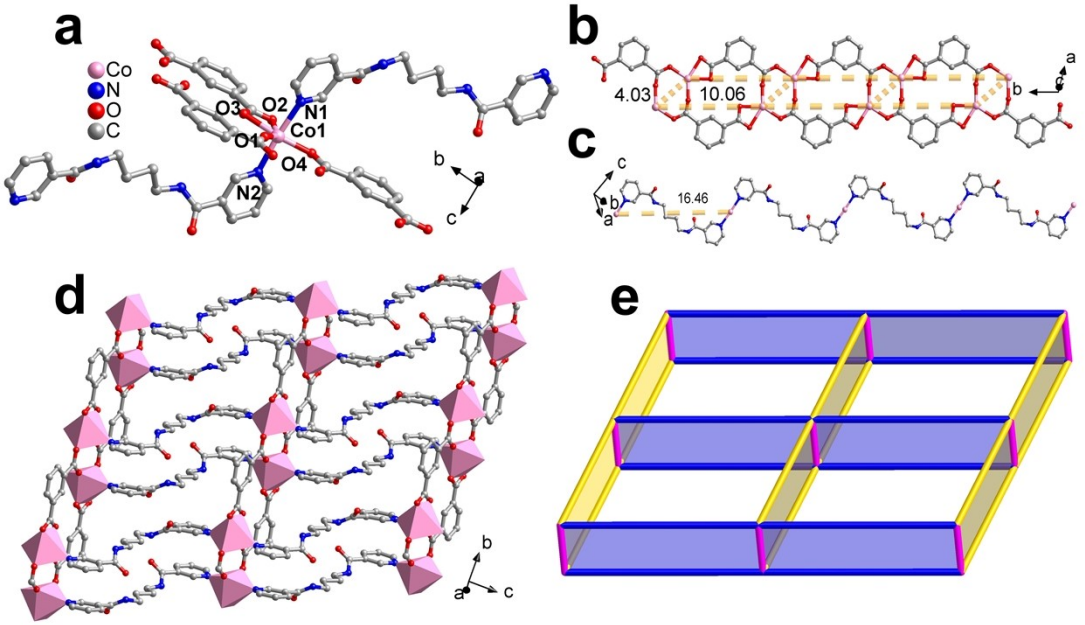

Fig. S1 (a) Coordination environment of the Co(II) ion in Co-MOF-H. (b) View of the 1D $[Co(1,3\text{-}BDC)]_{2n}$ chain. (c) The form of 3-dpyb linking 1D $[Co(3\text{-}dpyb)]_n$ chain. (d) 2D structure of Co-MOF. (e) Topological schematic of Co-MOF.

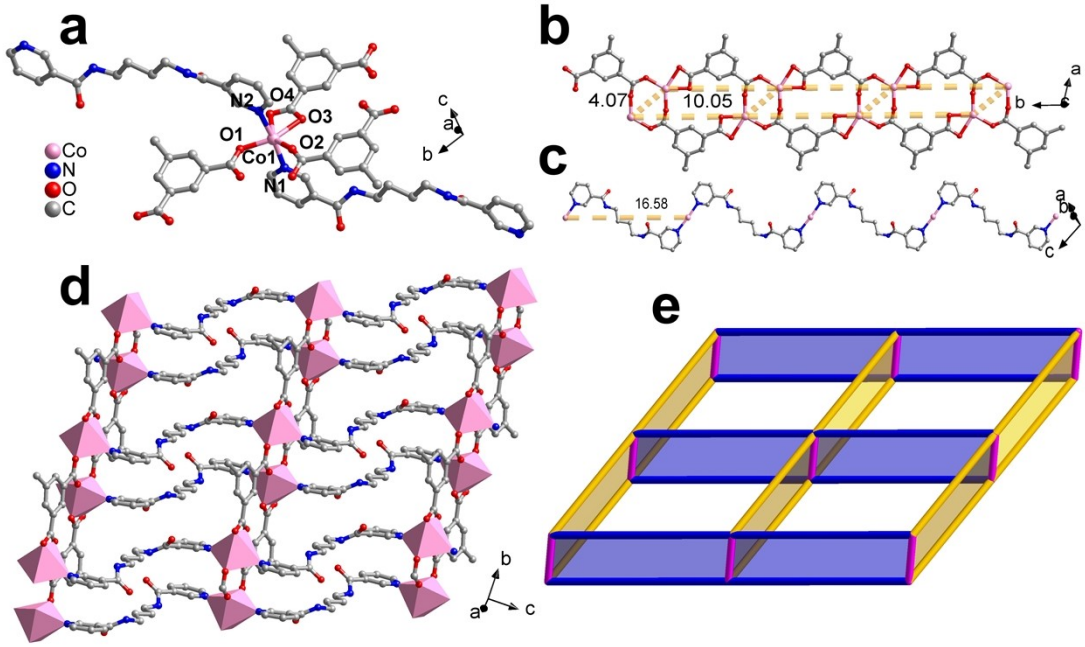

Fig. S2 (a) Coordination environment of the Co(II) ion in Co-MOF-CH_3. (b) View of the 1D $[Co(1,3\text{-}MIP)]_{2n}$ chain. (c) The form of 3-dpyb linking 1D $[Co(3\text{-}dpyb)]_n$ chain. (d) 2D structure of Co-MOF-CH_3. (e) Topological schematic of Co-MOF-CH_3.

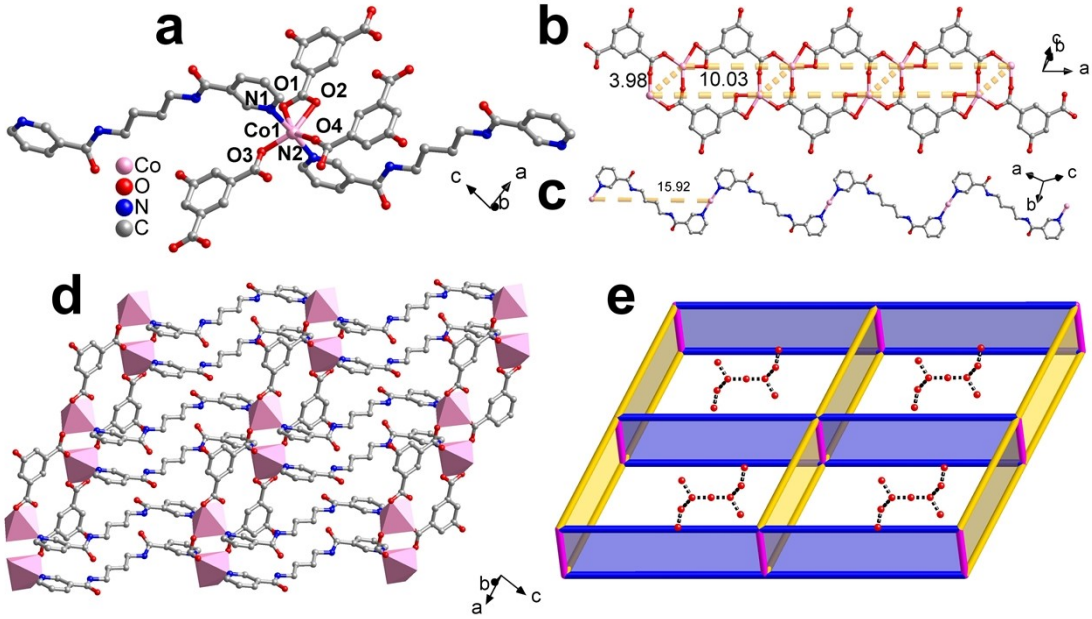

Fig. S3 (a) Coordination environment of the Co(II) ion in Co-MOF-OH. (b) View of the 1D $[Co(1,3\text{-}HIP)]_{2n}$ chain. (c) The form of 3-dpyb linking 1D $[Co(3\text{-}dpyb)]_n$ chain. (d) 2D structure of Co-MOF-OH. (e) Topological schematic of Co-MOF-OH.

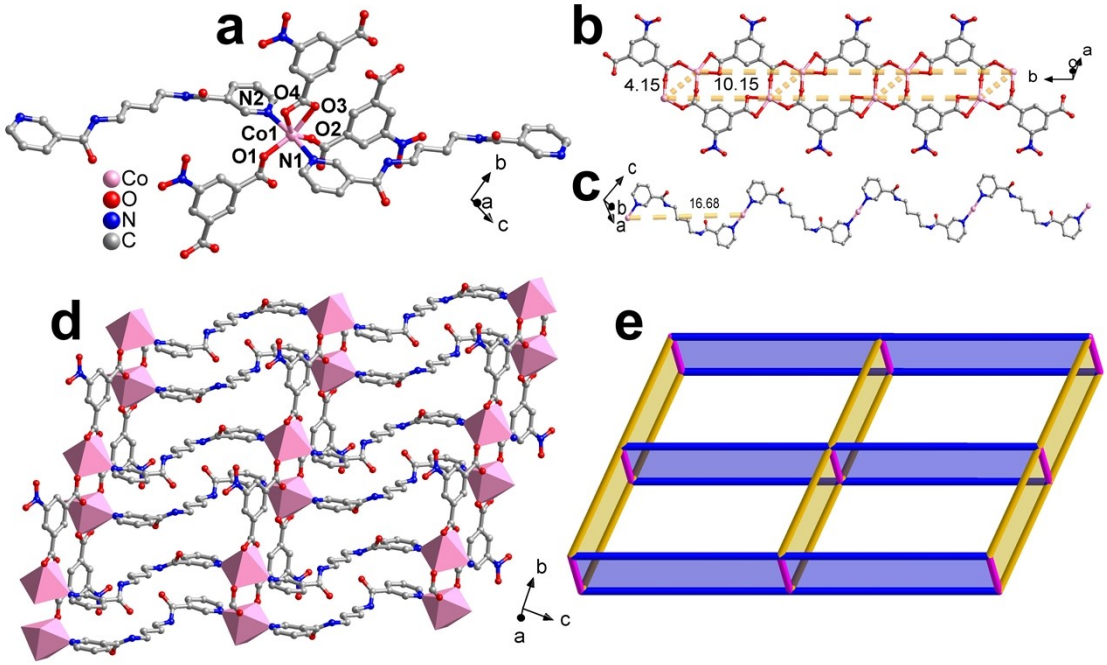

Fig. S4 (a) Coordination environment of the Co(II) ion in Co-MOF-NO_2. (b) View of the 1D $[Co(1,3\text{-}NIP)]_{2n}$ chain. (c) The form of 3-dpyb linking 1D $[Co(3\text{-}dpyb)]_n$ chain. (d) 2D structure of Co-MOF-NO_2. (e) Topological schematic of Co-MOF-NO_2.

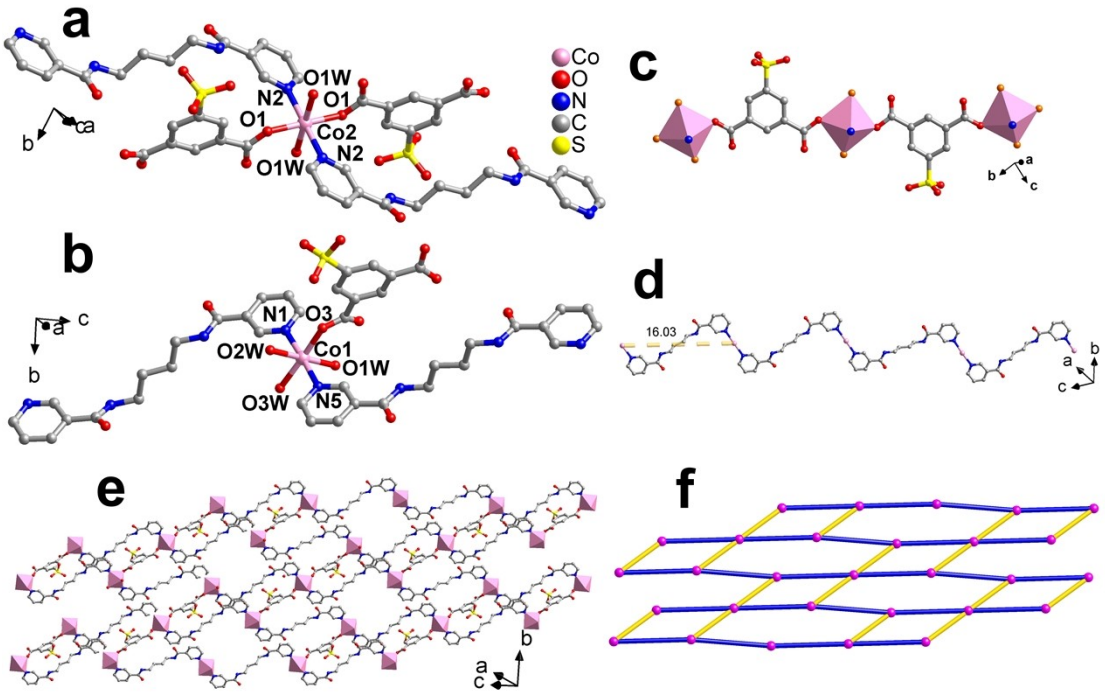

Fig. S5 (a and b) Coordination environment of the Co(II) ion in Co-MOF-SO_3. (c) View of the Co_3(5-SIP)$_2$ binuclear unit. (d) The form of 3-dpyb linking 1D [Co(3-dpyb)]$_n$ chain. (e) 2D structure of Co-MOF-SO_3. (f) Topological schematic of Co-MOF-SO_3.

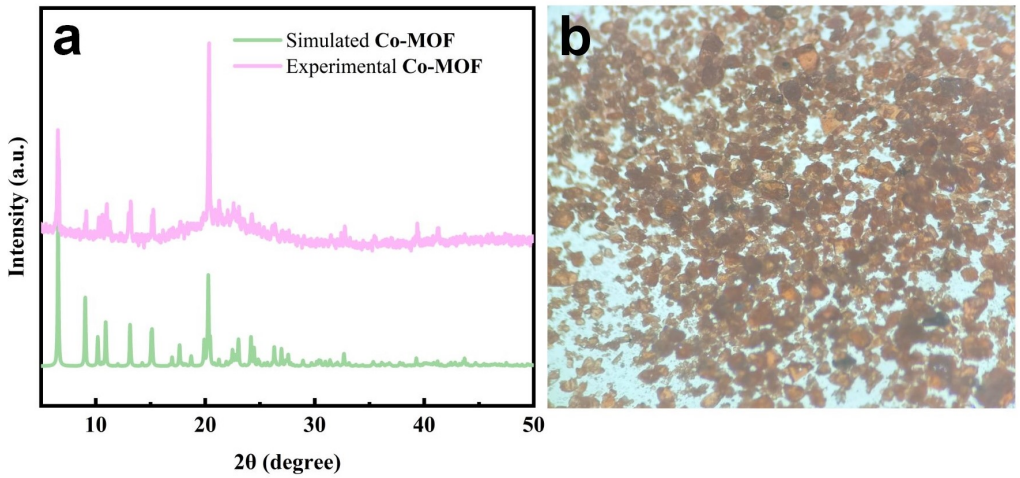

Fig. S6 (a) Comparison between XRD test data and simulation data of Co-MOF. (b) A photo of Co-MOF under an optical microscope.

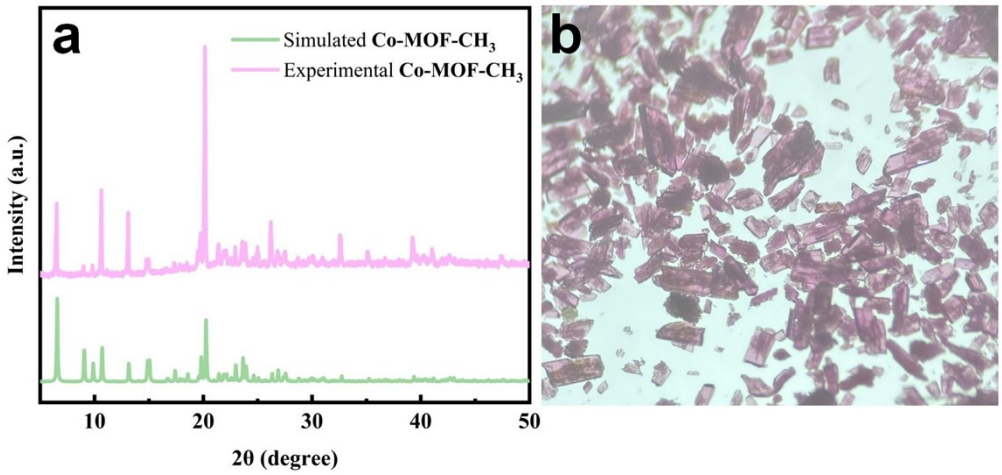

Fig. S7 (a) Comparison between XRD test data and simulation data of Co-MOF-CH_3. (b) A photo of Co-MOF-CH_3 under an optical microscope.

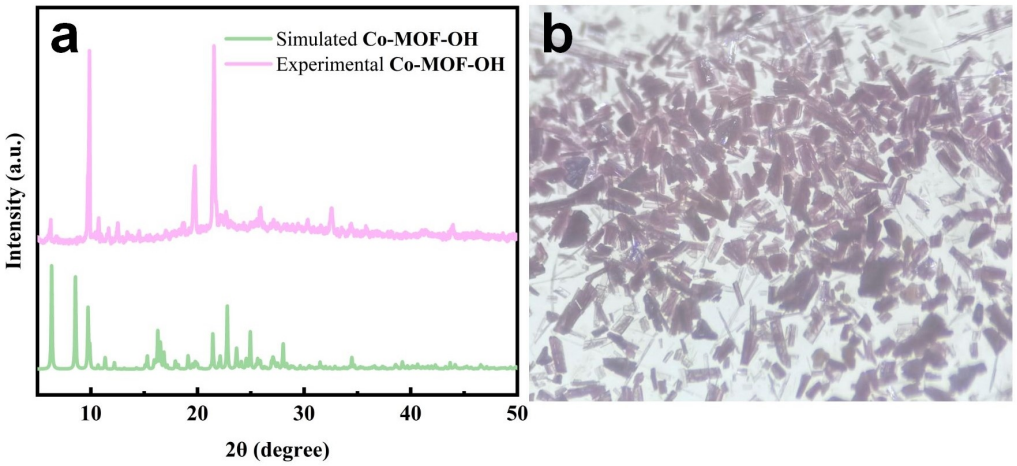

Fig. S8 (a) Comparison between XRD test data and simulation data of Co-MOF-OH. (b) A photo of Co-MOF-OH under an optical microscope.

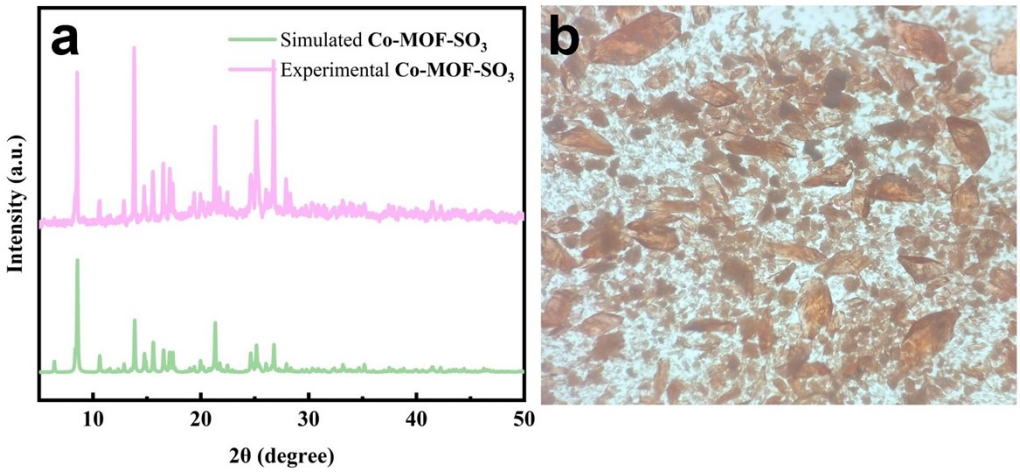

Fig. S9 (a) Comparison between XRD test data and simulation data of Co-MOF-SO_3. (b) A photo of Co-MOF-SO_3 under an optical microscope.

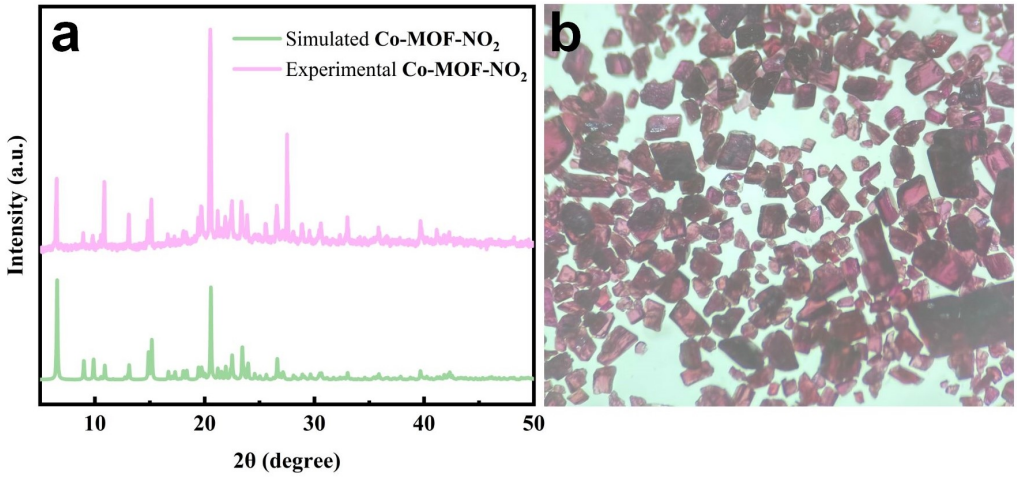

Fig. S10 (a) Comparison between XRD test data and simulation data of Co-MOF-NO_2. (b) A photo of Co-MOF-NO_2 under an optical microscope.

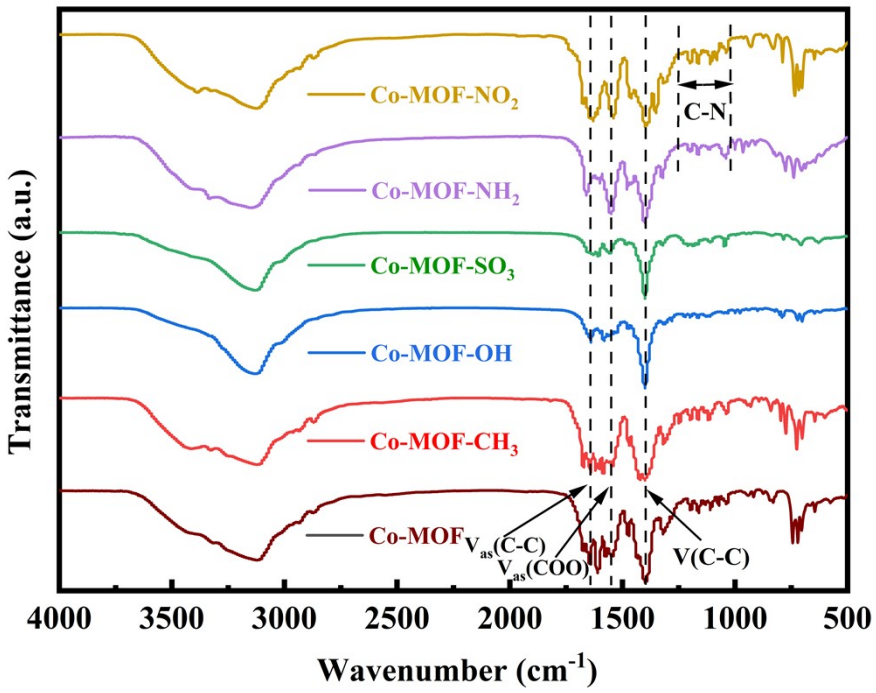

Fig. S11 FTIR spectra of Co-MOF series.

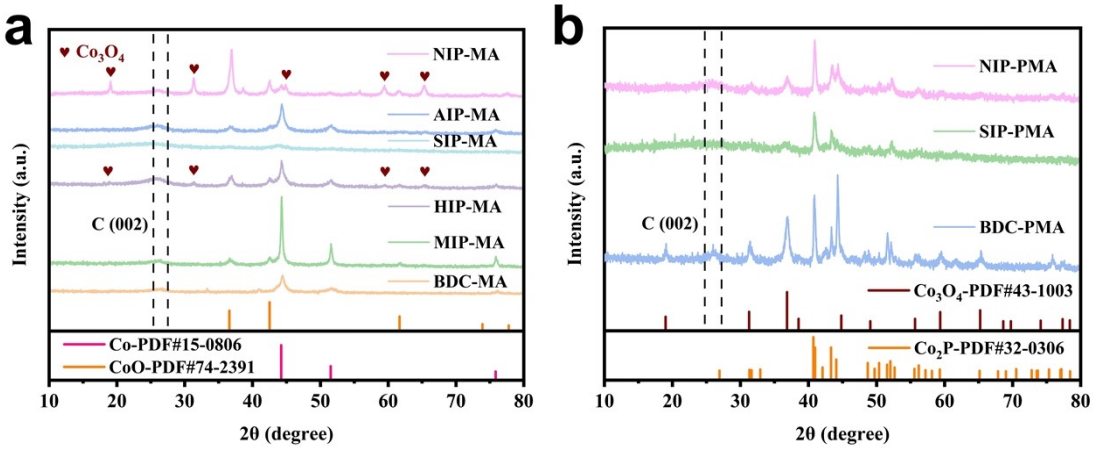

Fig. S12 PXRD patternd and phase analyses: (a) BDC-MA, MIP-MA, HIP-MA, SIP-MA, AIP-MA, NIP-MA; (b) BDC-PMA, SIP-PMA, NIP-PMA.

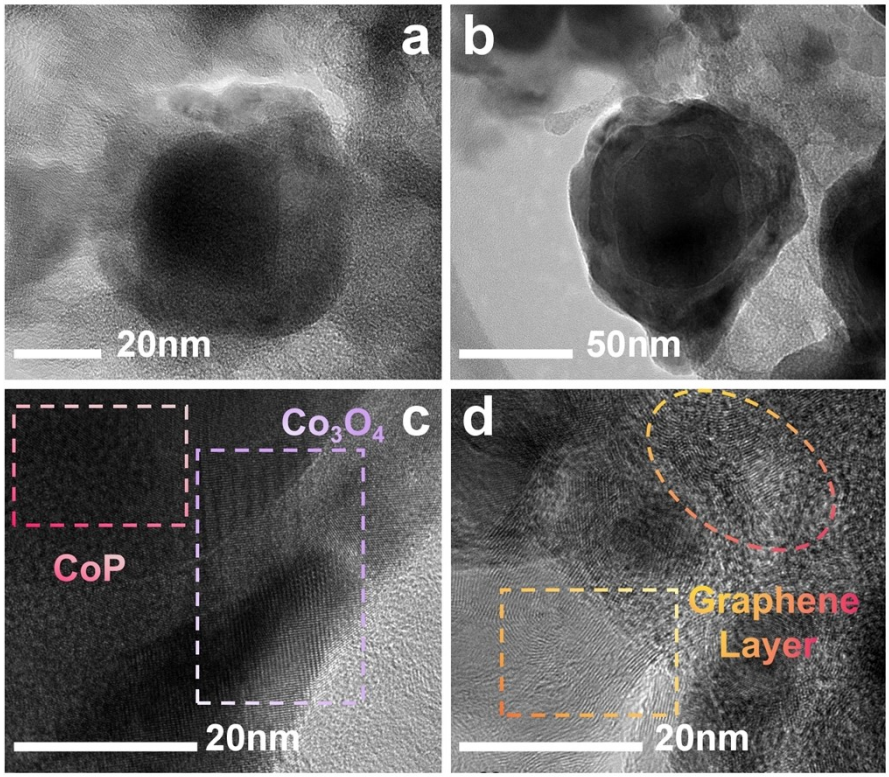

Fig. S13 (a and b) TEM images of AIP-PMA. (c and d) HRTEM images of AIP-PMA.

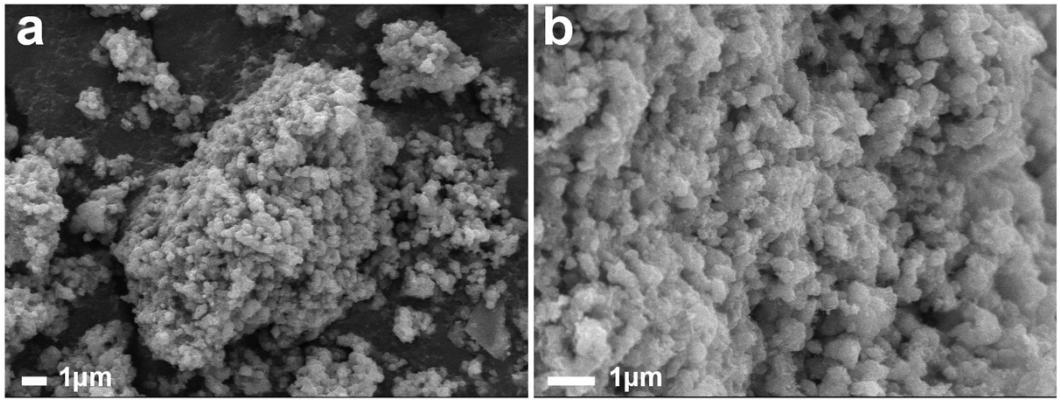

Fig. S14 SEM images of BDC-MA.

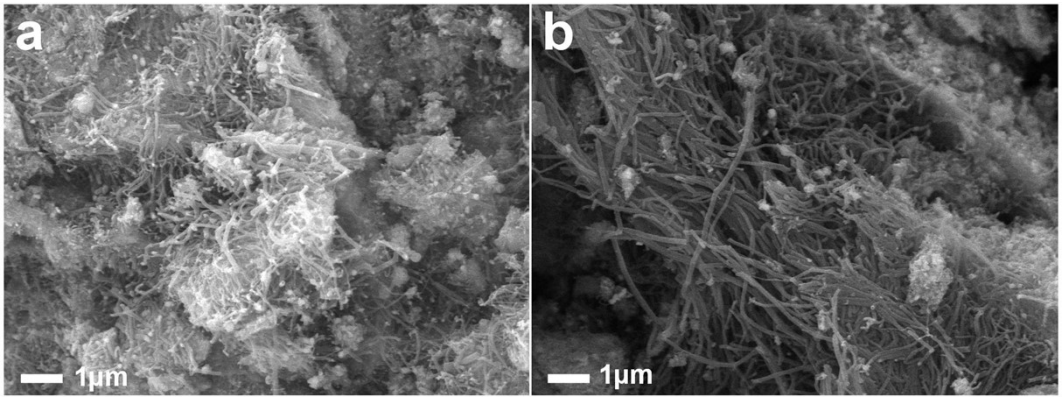

Fig. S15 SEM images of MIP-MA.

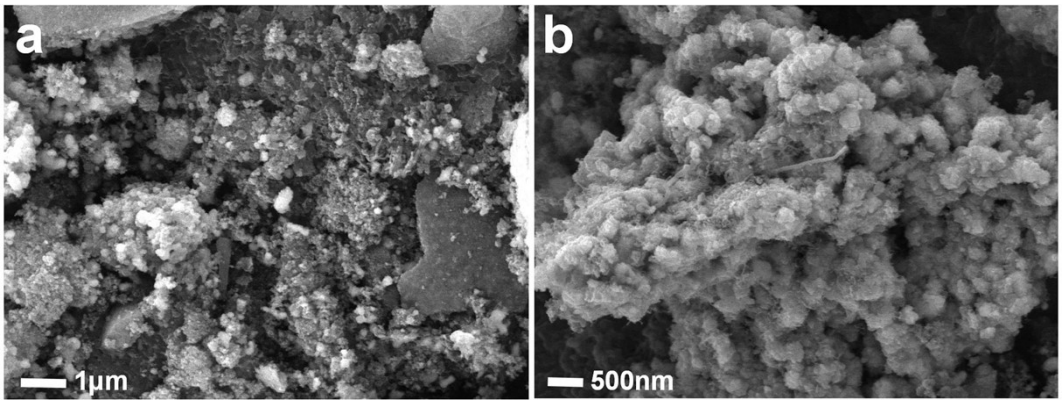

Fig. S16 SEM images of HIP-MA.

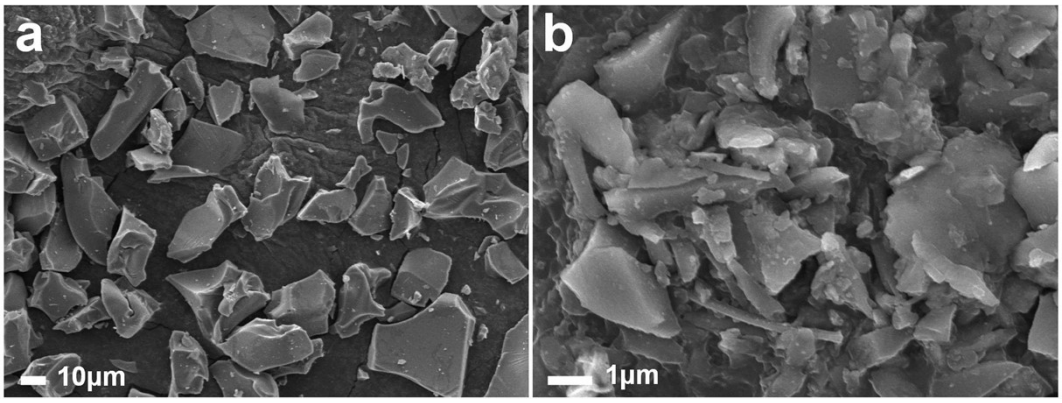

Fig. S17 SEM images of SIP-MA.

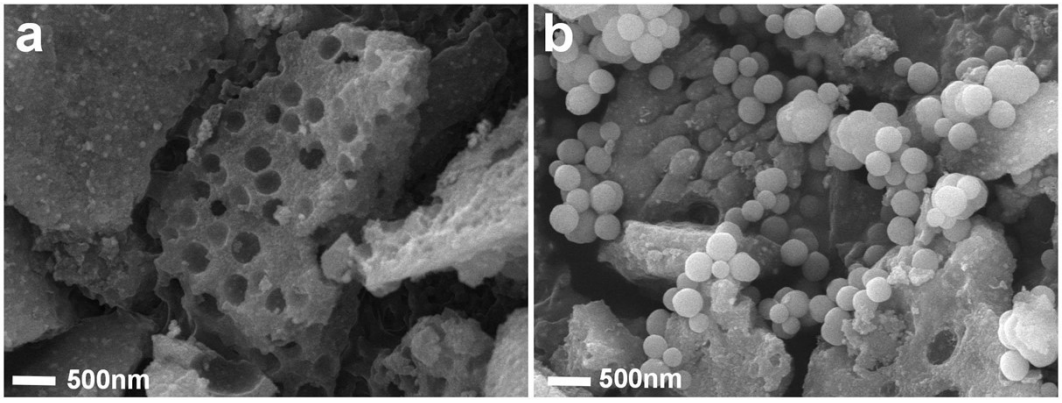

Fig. S18 SEM images of AIP-MA.

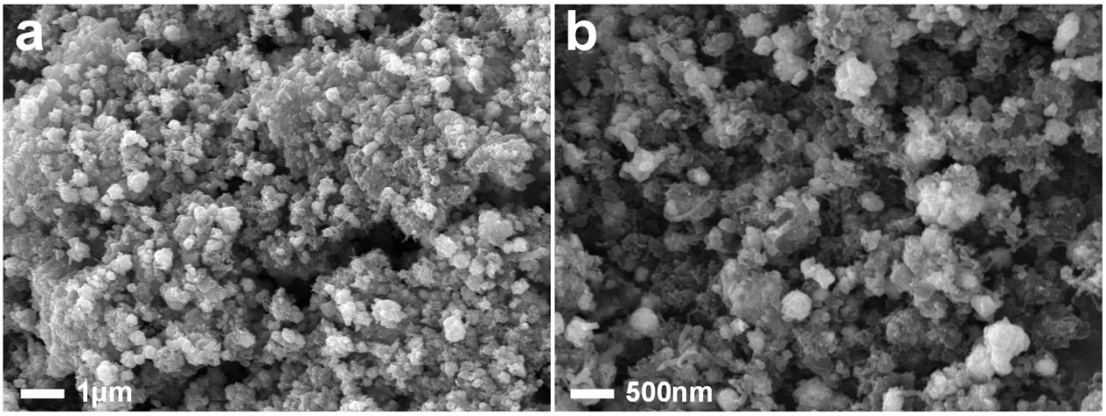

Fig. S19 SEM images of NIP-MA.

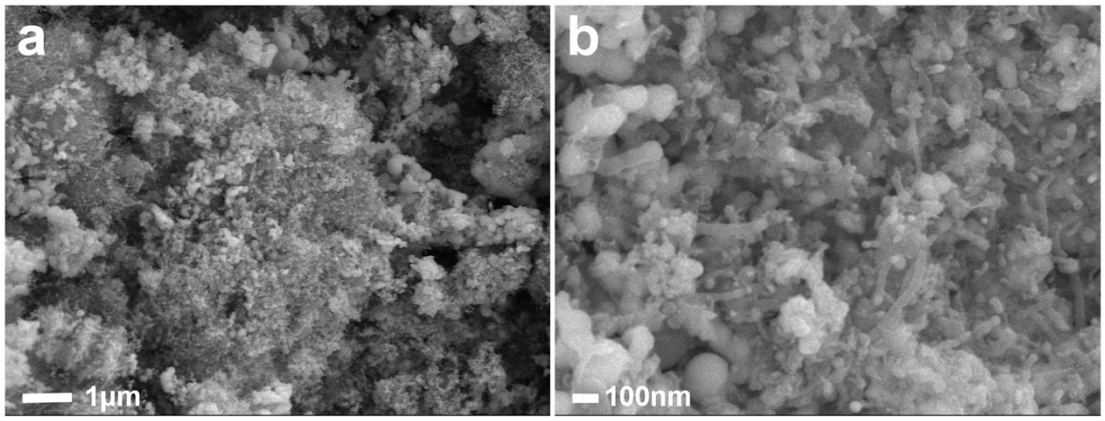

Fig. S20 SEM images of BDC-PMA.

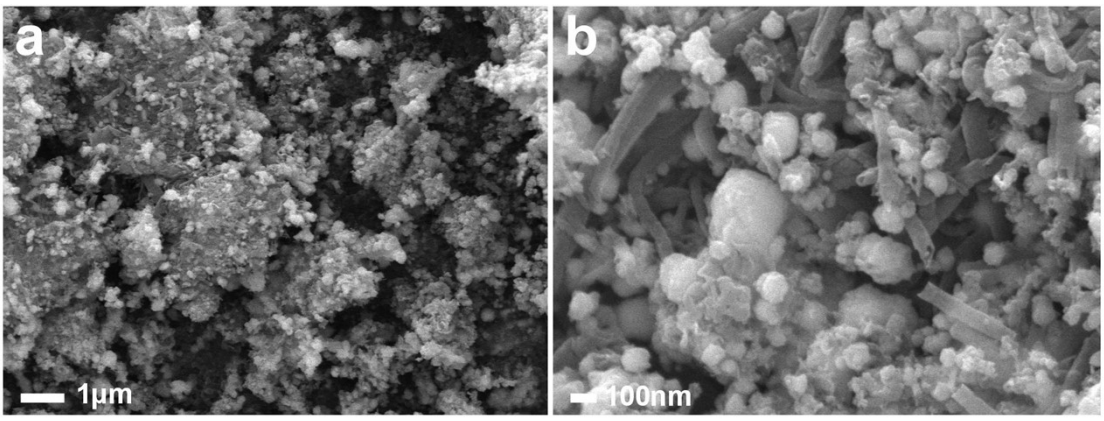

Fig. S21 SEM images of MIP-PMA.

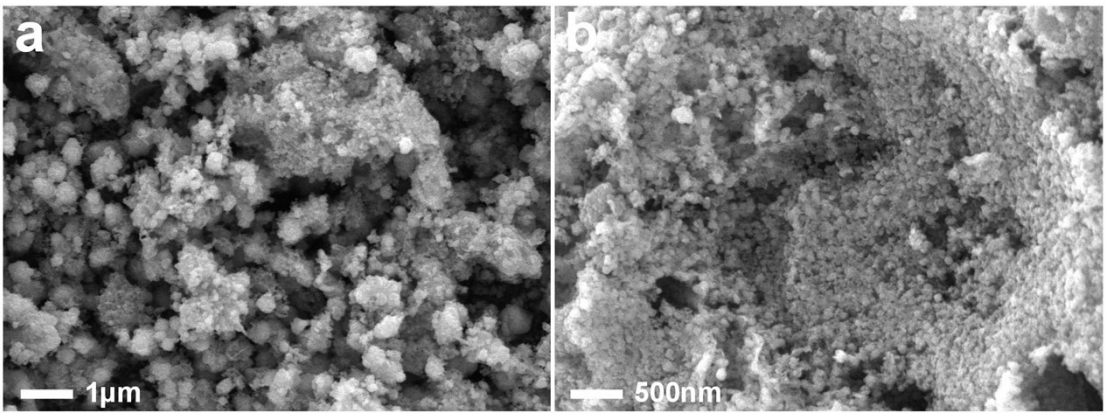

Fig. S22 SEM images of HIP-PMA.

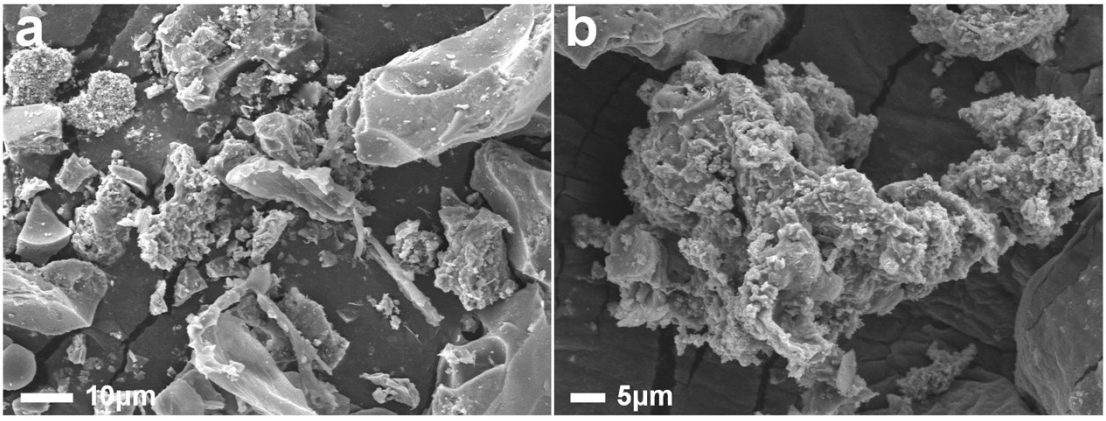

Fig. S23 SEM images of SIP-PMA.

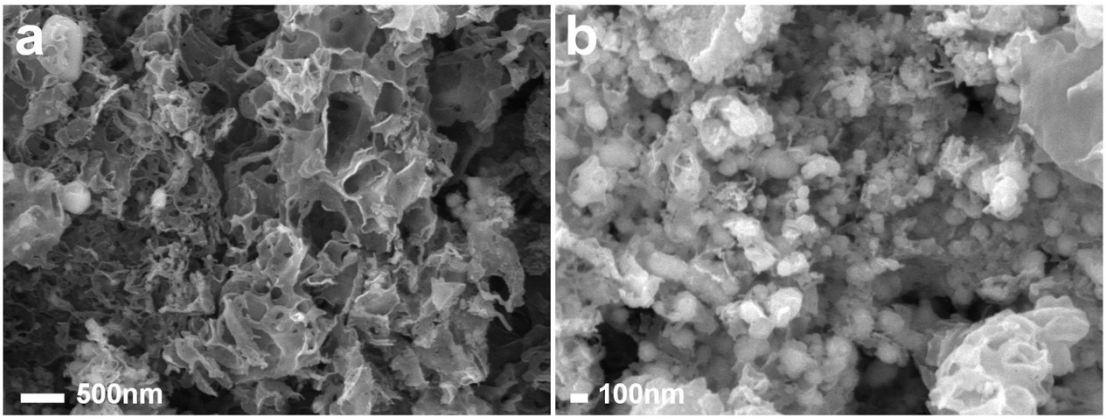

Fig. S24 SEM images of NIP-PMA.

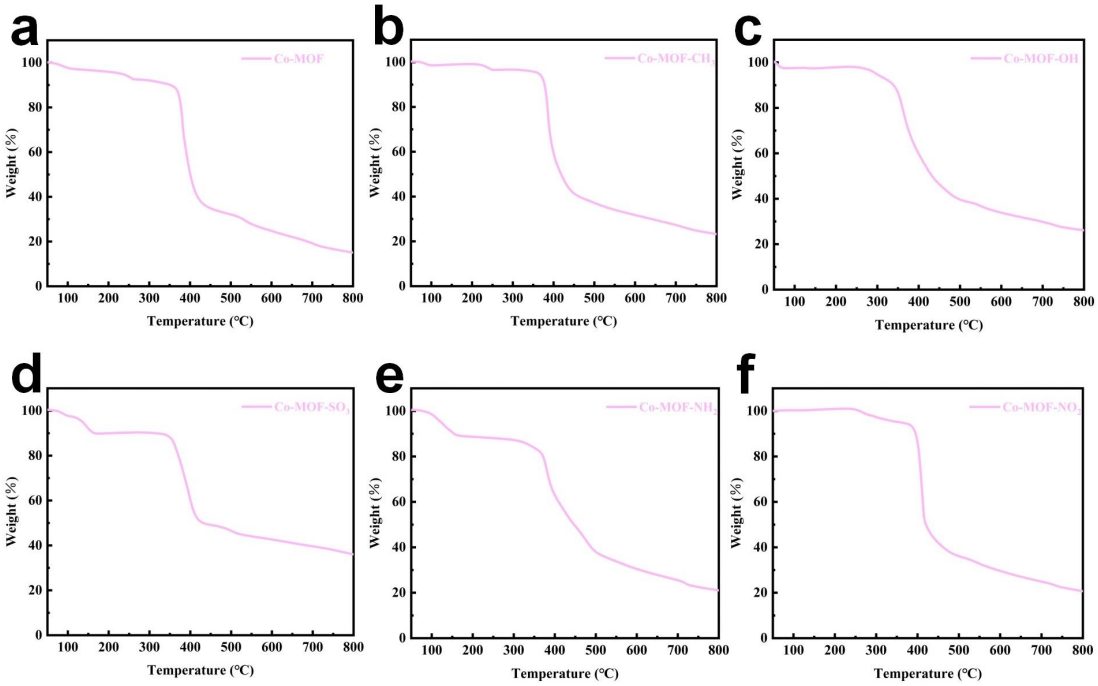

Fig. S25 Thermogravimetric analysis: (a) Co-MOF, (b) Co-MOF-CH_3, (c) Co-MOF-OH, (d) Co-MOF-SO_3, (e) Co-MOF-NH_2 and (f) Co-MOF-NO_2.

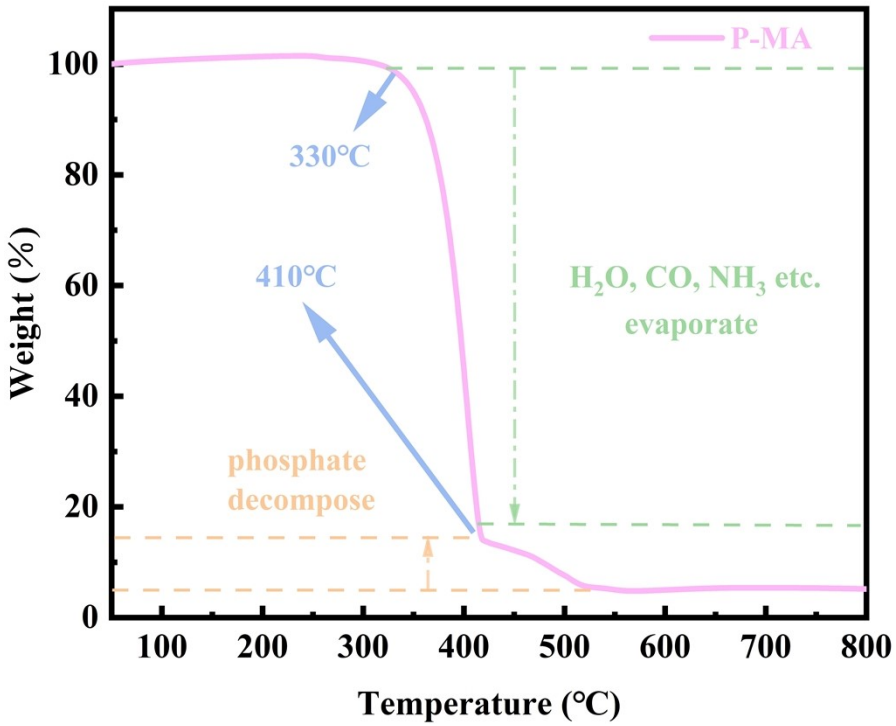

Fig. S26 Thermogravimetric analysis curve of melamine polyphosphate.

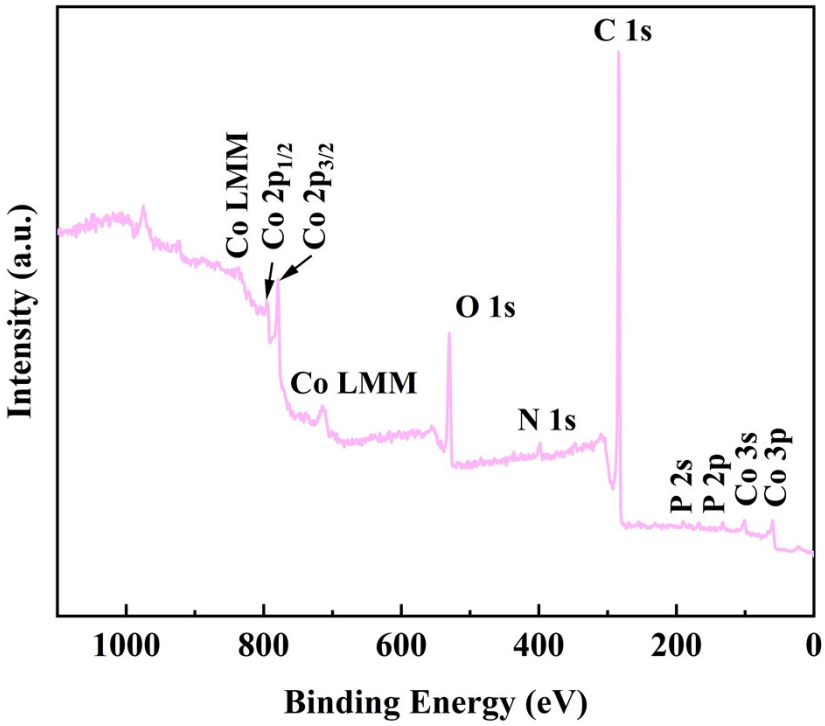

Fig. S27 XPS full spectrum of AIP-PMA.

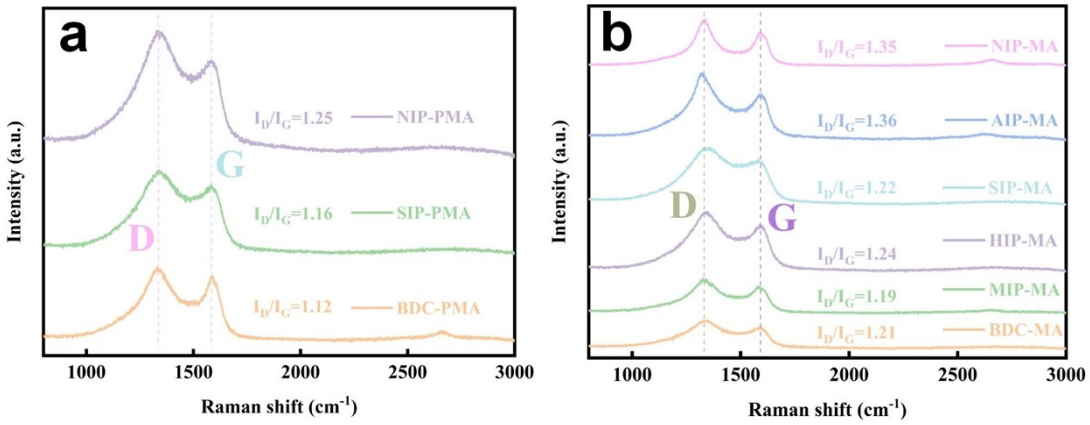

Fig. S28 Raman spectra: (a) BDC-PMA, SIP-PMA and NIP-PMA; (b) BDC-MA, MIP-MA, HIP-MA, SIP-MA, AIP-MA, NIP-MA.

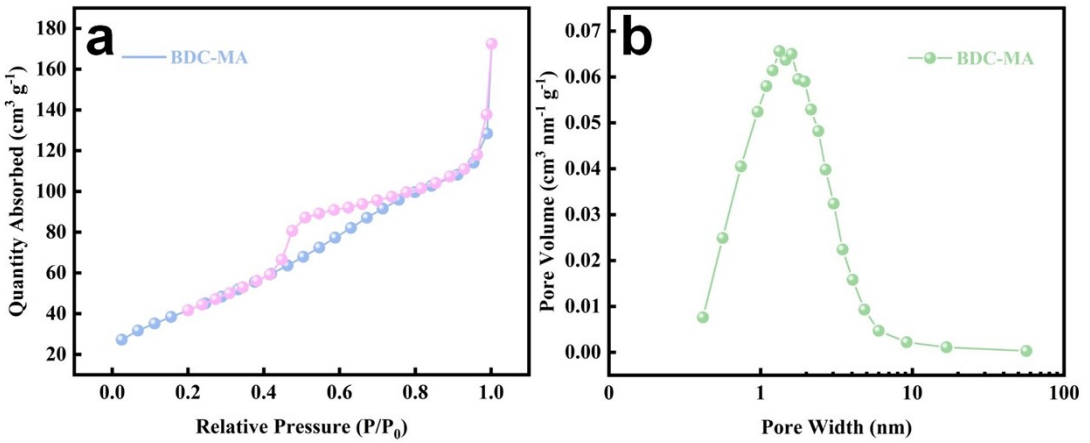

Fig. S29 (a) N_2 adsorption-desorption isotherms of BDC-MA. (b) The corresponding pore-size distribution plots for BDC-MA.

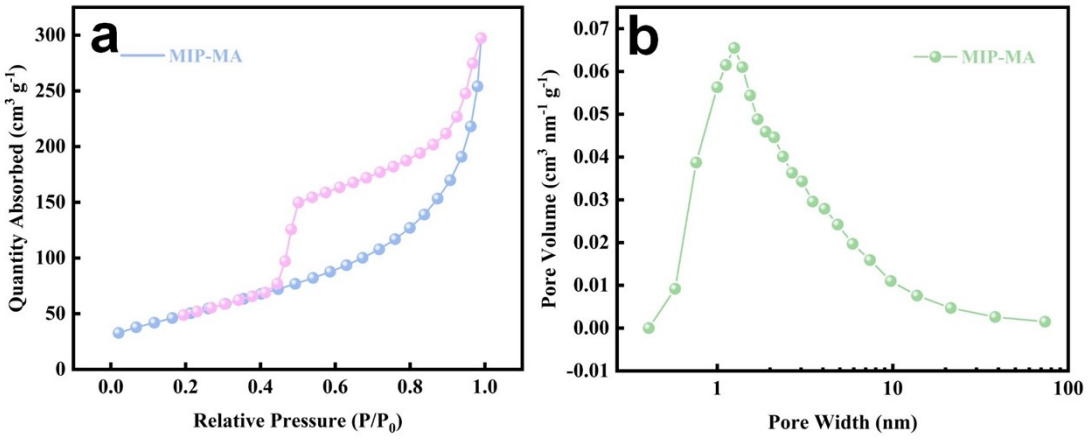

Fig. S30 (a) N_2 adsorption-desorption isotherms of MIP-MA. (b) The corresponding pore-size distribution plots for MIP-MA.

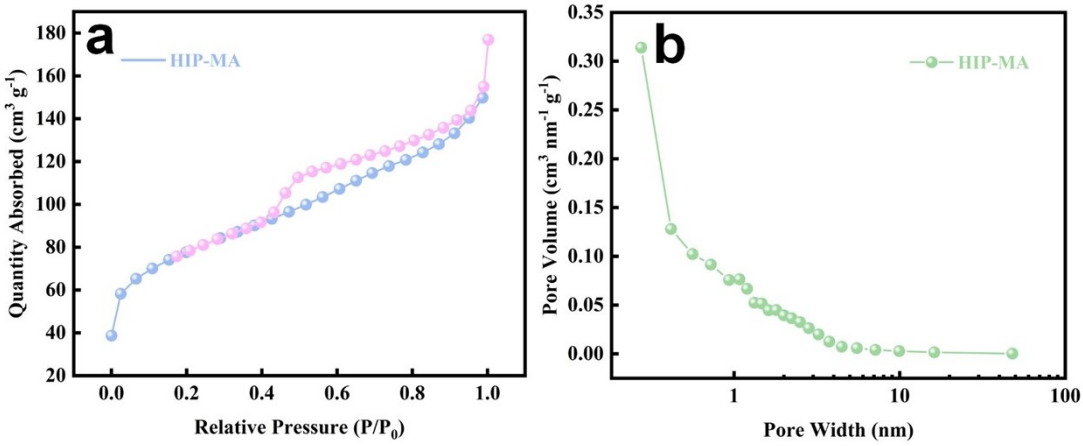

Fig. S31 (a) N_2 adsorption-desorption isotherms of HIP-MA. (b) The corresponding pore-size distribution plots for HIP-MA.

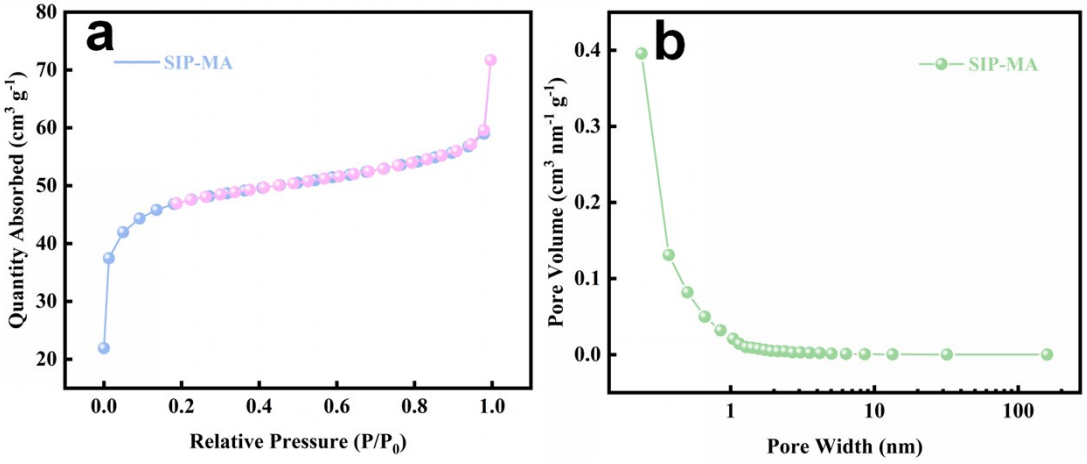

Fig. S32 (a) N_2 adsorption-desorption isotherms of SIP-MA. (b) The corresponding pore-size distribution plots for SIP-MA.

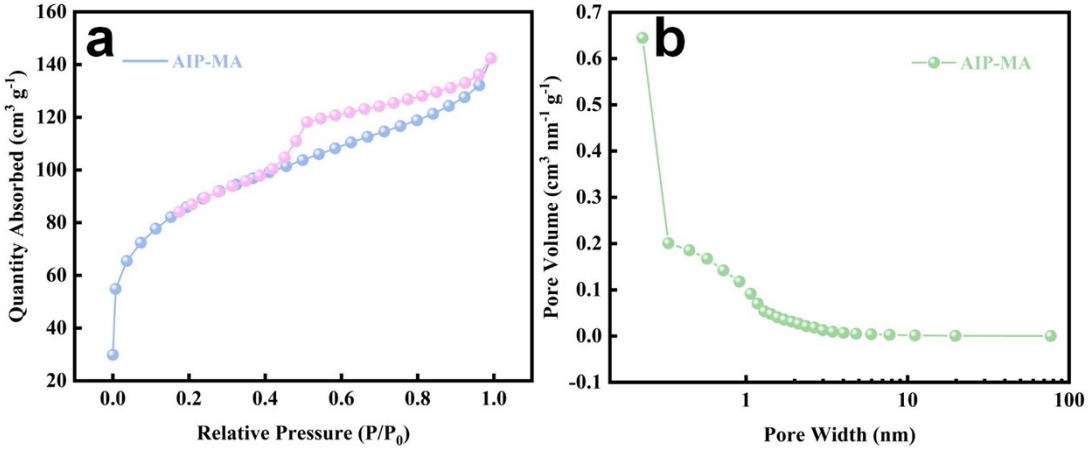

Fig. S33 (a) N_2 adsorption-desorption isotherms of AIP-MA. (b) The corresponding pore-size distribution plots for AIP-MA.

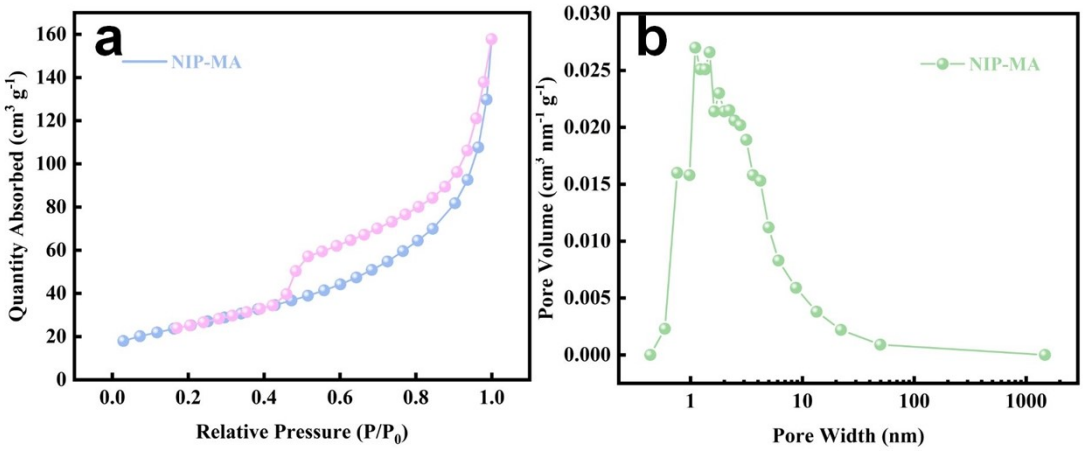

Fig. S34 (a) N_2 adsorption-desorption isotherms of NIP-MA. (b) The corresponding pore-size distribution plots for NIP-MA.

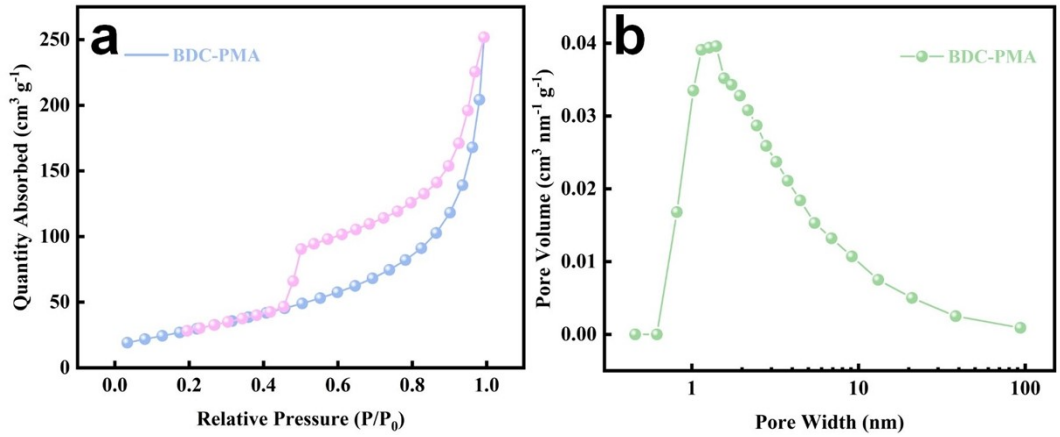

Fig. S35 (a) N_2 adsorption-desorption isotherms of BDC-PMA. (b) The corresponding pore-size distribution plots for BDC-PMA.

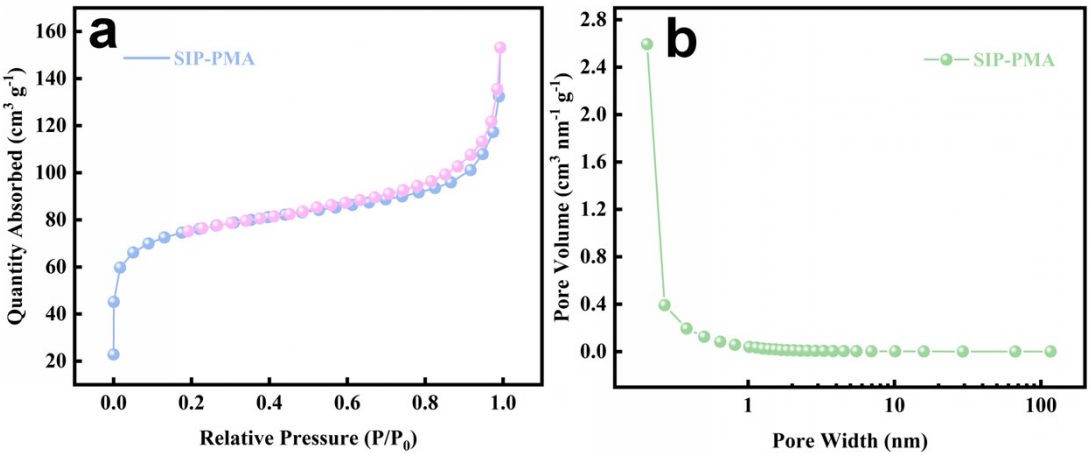

Fig. S36 (a) N_2 adsorption-desorption isotherms of SIP-PMA. (b) The corresponding pore-size distribution plots for SIP-PMA.

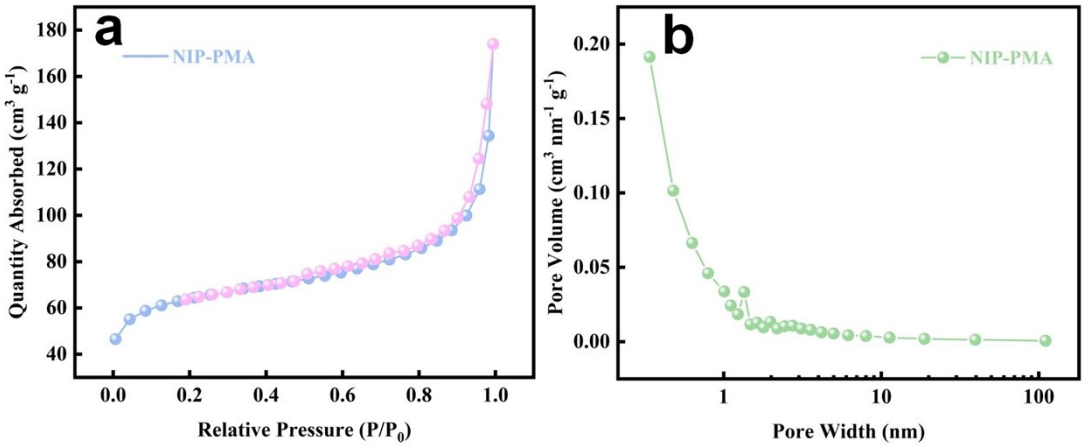

Fig. S37 (a) N_2 adsorption-desorption isotherms of NIP-PMA. (b) The corresponding pore-size distribution plots for NIP-PMA.

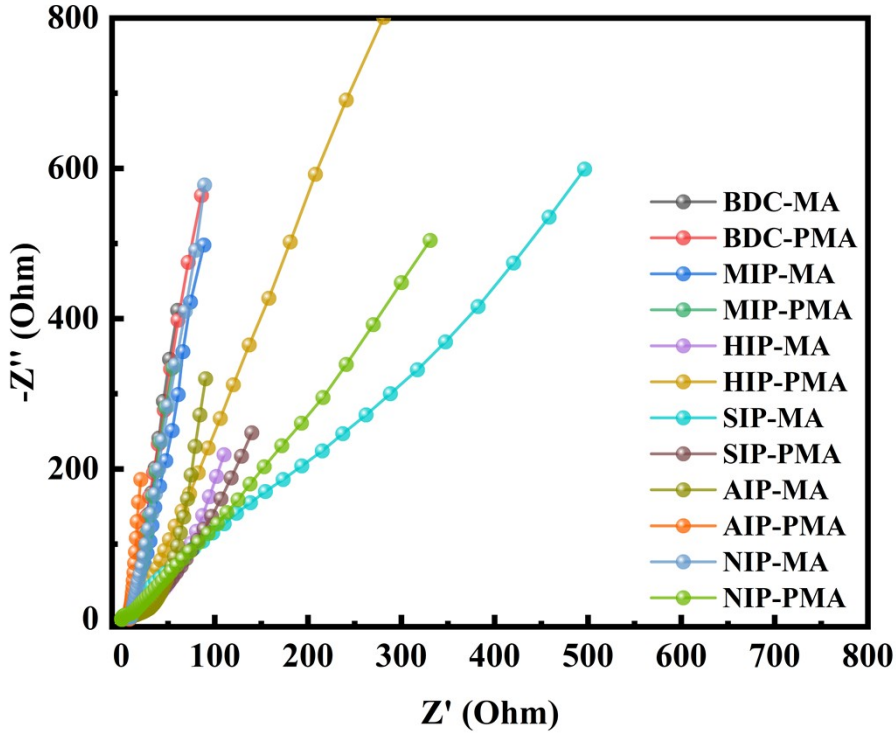

Fig. S38 EIS test of different samples.

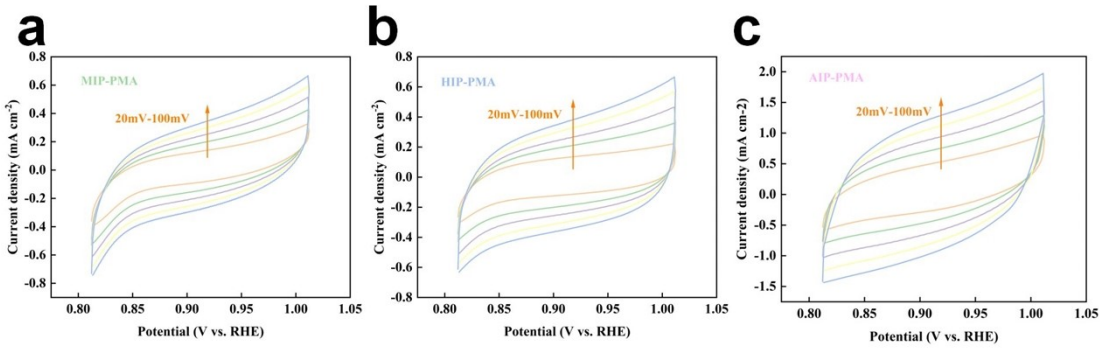

Fig. S39 CV curves of (a) MIP-PMA. (b) HIP-PMA and (c) AIP-PMA in 1 M KOH electrolyte for OER during the different scan rate of 20 mV–100 mV.

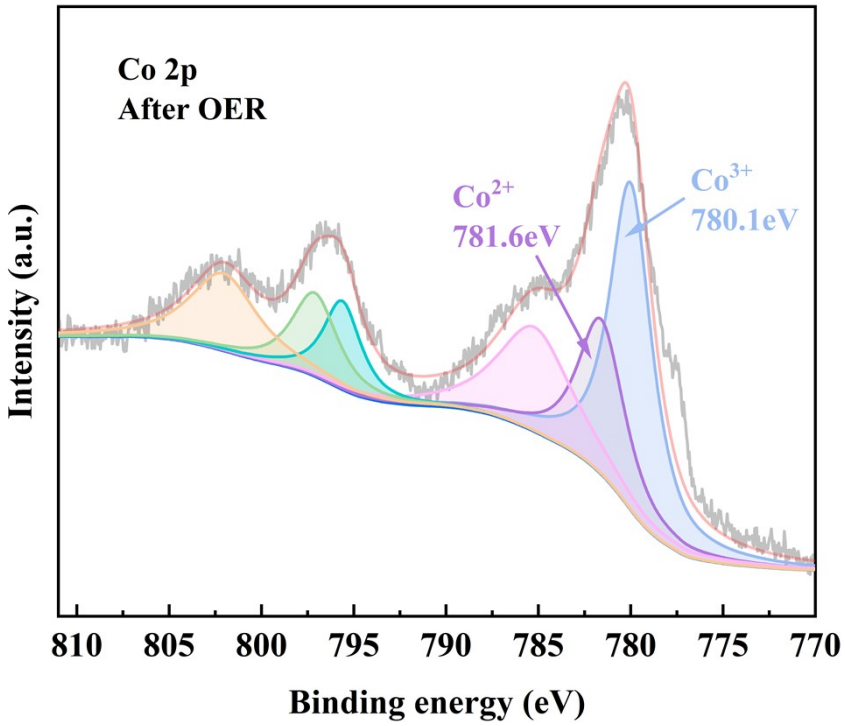

Fig. S40 XPS spectra of Co 2p for AIP-PMA after OER test.

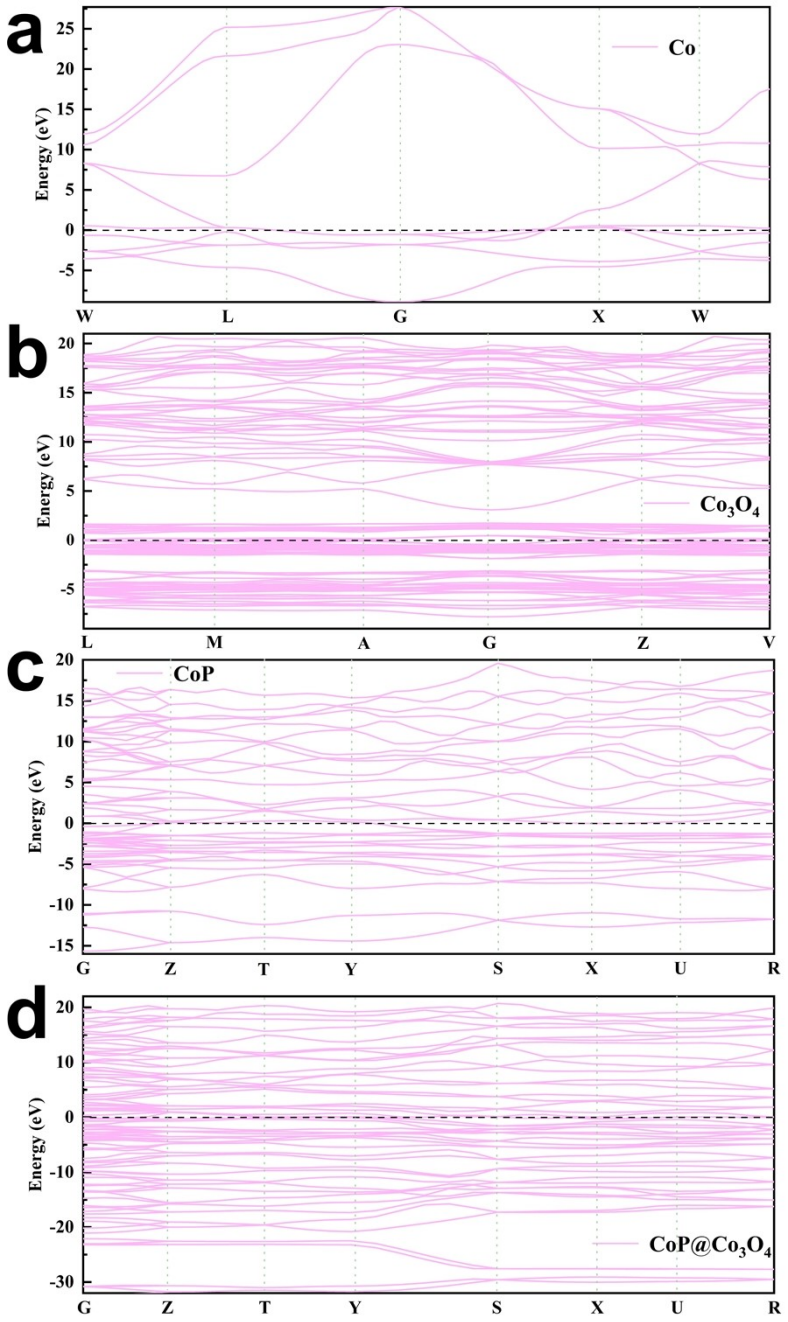

Fig. S41 Band structure of a) Co. b) Co_3O_4. c) CoP and d) $CoP@Co_3O_4$.

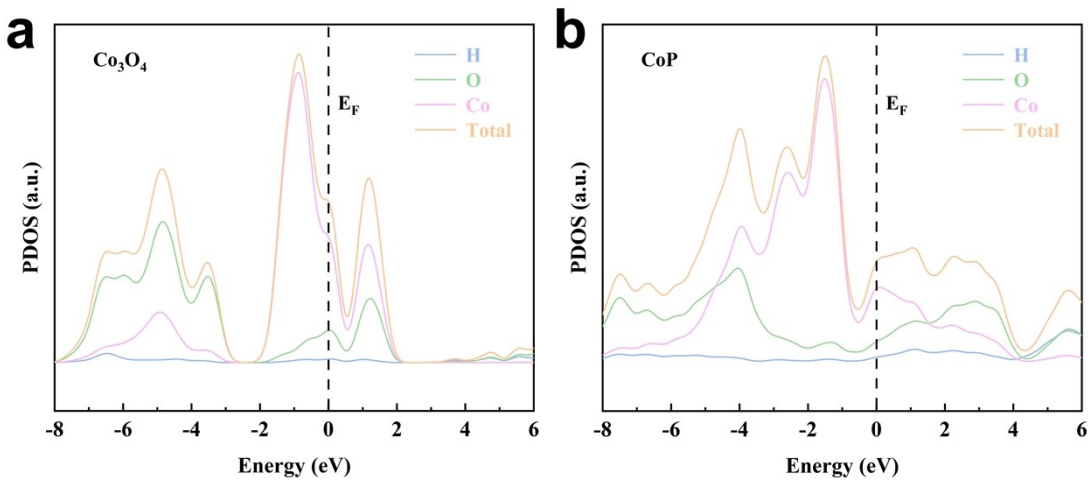

Fig. S42 PDOS of a) Co_3O_4 and b) CoP.

Table S1 Crystallographic data for Co-MOFs.

Co-MOF	Co-MOF-H	Co-MOF-CH_3	Co-MOF-NO_2	Co-MOF-OH	Co-MOF-SO_3	Co-MOF-NH_2
Empirical formula	$C_{24}H_{24}CoN_4O_7$	$C_{25}H_{26}CoN_4O_7$	$C_{24}H_{23}CoN_5O_9$	$C_{48}H_{66}Co_2N_8O_{25}$	$C_{64}H_{84}Co_3N_{12}O_{32}S_2$	$C_{16}H_{20}CoN_3O_8$
Formula weight	539.40	553.43	584.40	1272.95	1774.34	441.28
Crystal system	Triclinic	Triclinic	Triclinic	Triclinic	Triclinic	Triclinic
Space group	*P –1*	*P –1*	*P –1*	*P –1*	*P –1*	*P –1*
a (Å)	9.0683(6)	9.3600(17)	9.3224(7)	10.0267(6)	8.918(2)	8.4021(13)
b (Å)	10.0561(7)	10.0457(18)	10.1497(8)	11.4547(7)	14.271(3)	9.9042(15)
c (Å)	13.7972(10)	13.755(2)	13.7052(9)	14.3490(8)	16.111(4)	10.8986(16)
α (°)	93.6960(10)	92.924(5)	93.929(2)	78.351(2)	87.535(8)	82.684(4)
β (°)	100.9300(10)	100.746(5)	98.439(2)	79.389(2)	87.535(8)	84.928(4)
γ (°)	101.8910(10)	102.493(6)	103.119(2)	65.627(2)	74.767(7)	79.377(4)
V (Å ^{3})	1201.82(14)	1234.9(4)	1242.26(16)	1460.81(15)	1972.3(8)	882.2(2)
Z	2	2	2	1	1	2
D_c (g cm^{-3})	1.491	1.488	1.562	1.447	1.494	1.661
R_{int}	0.0148	0.0348	0.0652	0.0880	0.0221	0.0181
GOF	1.062	1.017	1.033	1.021	1.026	1.009
$R_1{}^a$ [$I > 2\sigma(I)$]	0.0433	0.0534	0.0840	0.0616	0.0524	0.0372
$wR_2{}^b$ (all data)	0.1183	0.1591	0.2568	0.1828	0.1826	0.1049

[a] $R_1 = \Sigma||F_o|-|F_c||/\Sigma|F_o|$, [b] $wR_2 = \Sigma[w(F_o^2-F_c^2)^2]/\Sigma[w(F_o^2)^2]^{1/2}$.

Table S2 Selected bond distances (Å) and angles (°) for Co-MOF-H.

Co(1)-O(4)#1	2.0321(19)	O(3)#2-Co(1)-N(2)#3	91.44(9)
Co(1)-O(1)	2.033(2)	O(4)#1-Co(1)-N(1)	87.01(9)
Co(1)-O(3)#2	2.141(2)	O(1)-Co(1)-N(1)	89.90(10)
Co(1)-N(2)#3	2.145(3)	O(3)#2-Co(1)-N(1)	93.49(9)
Co(1)-N(1)	2.155(3)	N(2)#3-Co(1)-N(1)	174.96(9)
Co(1)-O(2)#2	2.312(2)	O(4)#1-Co(1)-O(2)#2	89.09(8)
O(4)#1-Co(1)-O(1)	123.76(8)	O(1)-Co(1)-O(2)#2	146.97(8)
O(4)#1-Co(1)-O(3)#2	147.45(8)	O(3)#2-Co(1)-O(2)#2	58.42(7)
O(1)-Co(1)-O(3)#2	88.78(8)	N(2)#3-Co(1)-O(2)#2	93.25(9)
O(4)#1-Co(1)-N(2)#3	88.27(9)	N(1)-Co(1)-O(2)#2	88.44(9)
O(1)-Co(1)-N(2)#3	91.26(10)		

Symmetry codes: #1 -x+2, -y, -z+2; #2 -x+2, -y+1, -z+2; #3 x+1, y+1, z+1.

Table S3 Selected bond distances (Å) and angles (°) for Co-MOF-CH_3.

Co(1)-O(1)	2.0265(17)	O(3)#2-Co(1)-N(1)	90.25(8)
Co(1)-O(2)#1	2.0284(19)	O(1)-Co(1)-N(2)#3	86.44(8)
Co(1)-O(3)#2	2.1130(18)	O(2)#1-Co(1)-N(2)#3	89.00(9)
Co(1)-N(1)	2.143(2)	O(3)#2-Co(1)-N(2)#3	94.50(9)
Co(1)-N(2)#3	2.154(2)	N(1)-Co(1)-N(2)#3	174.80(8)
Co(1)-O(4)#2	2.352(2)	O(1)-Co(1)-O(4)#2	89.46(7)
O(1)-Co(1)-O(2)#1	122.19(8)	O(2)#1-Co(1)-O(4)#2	147.88(7)
O(1)-Co(1)-O(3)#2	147.51(8)	O(3)#2-Co(1)-O(4)#2	58.19(7)
O(2)#1-Co(1)-O(3)#2	90.30(8)	N(1)-Co(1)-O(4)#2	93.16(9)
O(1)-Co(1)-N(1)	88.42(8)	N(2)#3-Co(1)-O(4)#2	87.58(9)
O(2)#1-Co(1)-N(1)	93.08(9)		

Symmetry codes: #1 -x, -y-1, -z-1; #2 x, y-1, z; #3 x+1, y+1, z+1.

Table S4 Selected bond distances (Å) and angles (°) for Co-MOF-NO_2.

Co(1)-O(1)	2.031(4)	O(3)#2-Co(1)-N(1)	91.46(18)
Co(1)-O(2)#1	2.033(4)	O(1)-Co(1)-N(2)	85.61(19)
Co(1)-O(3)#2	2.138(4)	O(2)#1-Co(1)-N(2)	89.99(19)
Co(1)-N(1)	2.146(5)	O(3)#2-Co(1)-N(2)	93.78(19)
Co(1)-N(2)	2.154(5)	N(1)-Co(1)-N(2)	173.76(18)
Co(1)-O(4)#2	2.295(4)	O(1)-Co(1)-O(4)#2	93.97(15)
O(1)-Co(1)-O(2)#1	119.25(17)	O(2)#1-Co(1)-O(4)#2	146.36(16)
O(1)-Co(1)-O(3)#2	152.73(17)	O(3)#2-Co(1)-O(4)#2	58.80(15)
O(2)#1-Co(1)-O(3)#2	87.99(16)	N(1)-Co(1)-O(4)#2	92.54(18)
O(1)-Co(1)-N(1)	88.17(17)	N(2)-Co(1)-O(4)#2	87.29(18)
O(2)#1-Co(1)-N(1)	93.58(19)		

Symmetry codes: #1 -x+2, -y, -z+1; #2 x, y+1, z.

Table S5 Selected bond distances (Å) and angles (°) for Co-MOF-OH.

Co(1)-O(4)	2.011(3)	O(2)-Co(1)-N(1)	91.43(13)
Co(1)-O(3)	2.032(3)	O(4)-Co(1)-N(2)	89.76(13)
Co(1)-O(2)	2.123(3)	O(3)-Co(1)-N(2)	87.84(13)
Co(1)-N(1)	2.144(3)	O(2)-Co(1)-N(2)	92.00(13)
Co(1)-N(2)	2.151(3)	N(1)-Co(1)-N(2)	176.30(13)
Co(1)-O(1)	2.344(3)	O(4)-Co(1)-O(1)	148.33(11)
O(4)-Co(1)-O(3)	124.47(12)	O(3)-Co(1)-O(1)	87.11(10)
O(4)-Co(1)-O(2)	90.50(12)	O(2)-Co(1)-O(1)	57.92(10)
O(3)-Co(1)-O(2)	145.02(12)	N(1)-Co(1)-O(1)	91.58(12)
O(4)-Co(1)-N(1)	91.60(13)	N(2)-Co(1)-O(1)	89.07(12)
O(3)-Co(1)-N(1)	88.55(12)		

Table S6 Selected bond distances (Å) and angles (°) for Co-MOF-SO_3.

Co(1)-O(3)	2.0640(19)	O(3)-Co(1)-N(1)	92.44(9)
Co(1)-O(1W)	2.092(2)	O(1W)-Co(1)-N(1)	92.37(9)
Co(1)-O(2W)	2.093(2)	O(2W)-Co(1)-N(1)	87.87(9)
Co(1)-O(3W)	2.118(2)	O(3W)-Co(1)-N(1)	87.82(9)
Co(1)-N(5)	2.164(2)	N(5)-Co(1)-N(1)	177.45(8)
Co(1)-N(1)	2.179(2)	O(1)#1-Co(2)-O(1)	180.0
Co(2)-O(1)#1	2.0406(18)	O(1)#1-Co(2)-O(4W)	88.86(8)
Co(2)-O(4W)	2.151(2)	O(1)-Co(2)-O(4W)	91.14(8)
Co(2)-O(4W)#1	2.151(2)	O(1)#1-Co(2)-O(4W)#1	91.14(8)
Co(2)-N(2)#1	2.179(2)	O(1)-Co(2)-O(4W)#1	88.86(8)
Co(2)-N(2)	2.179(2)	O(4W)-Co(2)-O(4W)#1	180.0
O(3)-Co(1)-O(1W)	91.75(9)	O(1)#1-Co(2)-N(2)#1	88.96(9)
O(3)-Co(1)-O(2W)	87.70(9)	O(1)-Co(2)-N(2)#1	91.04(8)
O(1W)-Co(1)-O(2W)	179.41(9)	O(4W)-Co(2)-N(2)#1	92.94(8)
O(3)-Co(1)-O(3W)	176.16(10)	O(4W)#1-Co(2)-N(2)#1	87.06(8)
O(1W)-Co(1)-O(3W)	92.07(10)	O(1)#1-Co(2)-N(2)	91.04(9)
O(2W)-Co(1)-O(3W)	88.48(11)	O(1)-Co(2)-N(2)	88.96(9)
O(3)-Co(1)-N(5)	89.87(9)	O(4W)-Co(2)-N(2)	87.05(8)
O(1W)-Co(1)-N(5)	88.66(9)	O(4W)#1-Co(2)-N(2)	92.94(8)
O(2W)-Co(1)-N(5)	91.13(9)	N(2)#1-Co(2)-N(2)	180.0
O(3W)-Co(1)-N(5)	89.81(9)		

Symmetry codes: #1 -x+1, -y, -z+1.

Table S7 Selected bond distances (Å) and angles (°) for Co-MOF-NH_2.

Co(1)-O(1W)	2.1068(15)	O(4)#1-Co(1)-N(1)	91.53(6)
Co(1)-O(1)	2.1341(16)	O(1W)-Co(1)-N(3)#2	86.60(6)
Co(1)-O(4)#1	2.1458(15)	O(1)-Co(1)-N(3)#2	93.32(6)
Co(1)-N(1)	2.1516(18)	O(4)#1-Co(1)-N(3)#2	90.40(6)
Co(1)-N(3)#2	2.2514(17)	N(1)-Co(1)-N(3)#2	174.75(6)
Co(1)-O(3)#1	2.3007(15)	O(1W)-Co(1)-O(3)#1	86.30(6)
O(1W)-Co(1)-O(1)	131.99(6)	O(1)-Co(1)-O(3)#1	141.69(6)
O(1W)-Co(1)-O(4)#1	144.93(6)	O(4)#1-Co(1)-O(3)#1	58.64(6)
O(1)-Co(1)-O(4)#1	83.05(6)	N(1)-Co(1)-O(3)#1	89.58(6)
O(1W)-Co(1)-N(1)	89.01(7)	N(3)#2-Co(1)-O(3)#1	87.26(6)
O(1)-Co(1)-N(1)	91.76(7)		

Symmetry codes: #1 x, y+1, z; #2 -x+2, -y, -z.

Table S8 Comparison of OER performance for some Co-based electrocatalysts reported in 1M KOH solution.

Catalyst	Electrode	η_{10} (mV)	Tafel slope (mV dec^{-1})	Reference
Co_2P/CoNPC	GC	328	78	*Adv. Mater.* 2020, **32**, 2003649
CoMe	GC	350	116.7	*Adv. Funct. Mater.* 2021, **31**, 2009245
Co-C_3N_4/CNT	RRDE	380	82	*Adv. Mater.* 2020, **32**, 2003134
Co-Mo_2C-CN_x-2	GC	338	70	*Appl. Catal. B: Environ.* 2021, **284**, 119738
CoBDC	$BiVO_4$	400	80	*ACS Nano* 2022, **16**, 9523
MOF-Fe/Co	GC	427	156	*Angew. Chem. Int. Ed.* 2021, **60**, 12097
Co_2P/Mo_3Co_3C/Mo_2C@C	GC	362	82	*J. Mater. Chem. A*, 2018, **6**, 5789
CoP_3 CPs	CP	343	76	*Phys. Chem. Chem. Phys.* 2017, **19**, 2104.
M-MoS_2@Co	GC	370	90	*Environ.Energy Mater.* 2024, 10. 1002/eem2.12702
Mo-Co_3O_4 NFs	GC	362	96.2	*Adv. Funct. Mater.* 2022, **32**, 2107382
CoP@Co_3O_4/N-doped graphene	GC	320	78.9	This work

Reference

1 X. L. Wang, J. Luan, H. Y. Lin, Q. L. Lu, C. Xu and G. C. Liu, *Dalton Trans.* 2013, **42**, 8375-8386.

2 G. M. Sheldrick, *Acta Crystallogr. Sect. A: Found. Crystallogr.* 2008, **64**, 112-122.

3 J. P. Perdew, K. Burke and M. Ernzerhof, *Phys. Rev. Lett.* 1996, **77**, 3865.

4 B. Hammer, L. B. Hansen and J. K. Nørskov, *Phys. Rev. B* 1999, **59**, 7413.

5 J. K. Nørskov, J. Rossmeisl, A. Logadottir, L. Lindqvist, J. R. Kitchin, T. Bligaard and H. Jonsson, *J. Phys. Chem. B*, 2004, **108**, 17886.